FAILURE OF BUTTERFLY SPECIMENS UNDER MIXED LOADING

Larbi Siad
Université de Reims, Moulin de la Housse 51687 Reims, France, larbi.siad@univ-reims.fr

Keywords : ductile damage, low stress triaxiality, microvoids, simulation, third invariant.

Abstract

An extended version of the well-known GTN isotropic hardening model is proposed in this paper. The yield function of the proposed constitutive model possesses the distinctiveness to explicitly depend upon the third stress invariant. Besides, the Tvergaard parameters depend upon the void volume fraction. The proposed constitutive model is used to numerically analyze the failure behaviour of butterfly specimen. As long as softening initiation of specimen is not reached, the computational results highlight similarities and good agreement with those provided by the use of the GTN model. These observations hold for tension-dominated deformation and shear-dominated deformation as well. However, for the later loading, discrepancy shows up as soon as specimen failure starts.

1 Introduction

This investigation addresses the use of an extended version of the GTN isotropic hardening model to analyse the ductile failure behaviour of butterfly specimen subjected to combined shear and tension large deformations. To put it in a nutshell, for the GTN model material [3] is assumed to be composed of a dense elastic-plastic matrix sprinkle with evenly distributed spherical microvoids. As regard failure behaviour, when the stress triaxiality (the ratio of the first to second stress invariants) is high enough, the voids remain near spherical and, as a matter of fact, the ductile fracture process is rather well described by the GTN model. On the other hand, if void nucleation is disregarded, this model cannot describe ductile damage evolution for shear-dominated loading. For such a loading for which stress triaxiality is low and even zero in case of pure shear, continued softening leading to ductile failure is known to occur [4].
An extension of the Gurson-Tvergaard's plastic potential was proposed in [7] where the authors focused their study on the determination of yield surfaces for porous plastic materials using a huge number of finite element simulations. The porous ductile materials contain spherical empty voids arranged in cubic arrays, *namely*, simple cubic (SC), Body-Centred Cubic (BCC) and Face-Centred Cubic (FCC) arrays. FEA was used to simulate unit cells and the macroscopic yield surfaces of the porous materials were obtained using the probing technique which goal is to obtain a yield function in an analytical expression that can be used in continuum studies. For more detailed explanations of the subject, the reader are referred to the paper [7]. The obtained yield points was fitted by a new yield function which turned out to be similar to the Gurson-Tvergaard one for porosity ranging between a very small value to the percolation threshold. This yield function was found to explicitly depend upon the third stress invariant.
A constitutive GTN-like model based on the proposed plastic potential is numerically implemented in a FE program. The presence of the third stress invariant in the yield function typically results in a high degree of non-linearity. The constitutive equations and the coalescence criterion based on the effective porosity are integrated using the general backward-Euler return algorithm [2]. This stress integration algorithm has been developed and implemented into Abaqus/Explicit. Subsequently, the proposed model constructed in this way is then used to analyze the behavior of a three-dimensional optimized butterfly specimen [6] subjected to shear-dominated and tension-dominated deformation, resulting in low and high stress triaxialities in the middle section of the specimen, respectively.

2 Constitutive relations

❶ Approximate GT-like condition proposed in [7] :

$$\begin{aligned}\Phi(\boldsymbol{\sigma};\mathbf{H};s) = \; & \left(\frac{q}{\bar{\sigma}}\right)^2 + 2\,a_1(f)\,\cosh\left(-\frac{3\,a_2(f)\,p}{2\,\bar{\sigma}}\right) - 1 - a_1(f)^2 \\ & + s(f)\,\frac{p}{\bar{\sigma}}\left(\frac{\mathrm{I}_3}{\bar{\sigma}^3} + \frac{p^3}{\bar{\sigma}^3} + \frac{1}{3}\,\frac{p}{\bar{\sigma}}\left[2\,a_1(f)\cosh\left(-\frac{3\,a_2(f)\,p}{2\bar{\sigma}}\right) - 1 - a_1(f)^2\right]\right) = 0\end{aligned} \tag{1}$$

(a) The determinants $\mathrm{I}_3 := \det(\boldsymbol{\sigma})$ and $J_3 := \det \boldsymbol{\sigma}'^3$ are related by $I_3 = J_3 + \frac{1}{3}\,p\,q^2 - p^3$.

(b) The macroscopic Cauchy stress tensor $\boldsymbol{\sigma}$ is resolved as $\boldsymbol{\sigma} = -p\mathbb{1} + \frac{2}{3}\,q\,\mathbf{n}$ with $\mathbf{n} = \frac{3}{2}\frac{\boldsymbol{\sigma}'}{q}$ where $p = -\frac{1}{3}\,\mathrm{tr}\,\boldsymbol{\sigma}$ is the hydrostatic pressure, $\mathbb{1}$ is the second order identity tensor, $\boldsymbol{\sigma}'$ is the deviatoric stress tensor, and $q = \left(\frac{3}{2}\,\boldsymbol{\sigma}' : \boldsymbol{\sigma}'\right)^{1/2}$ is the von Mises stress.

(c) $\bar{\sigma}$ is the effective flow stress of the damage-free matrix material, (q_1, q_2) are the Tvergaard parameters, and $\mathbf{H} = (\bar{\epsilon}^p, f)$ where $\bar{\epsilon}^p$ is the effective plastic strain.

❷ Constitutive equations written in a rate format :

$$\dot{\boldsymbol{\epsilon}} = \dot{\boldsymbol{\epsilon}}^e + \dot{\boldsymbol{\epsilon}}^p \;,\; \dot{\boldsymbol{\sigma}} = \mathbf{C}^e : (\dot{\boldsymbol{\epsilon}} - \dot{\boldsymbol{\epsilon}}^p) \;,\; \dot{\boldsymbol{\epsilon}}^p = \dot{\lambda}\,\mathbf{r}(\boldsymbol{\sigma};\mathbf{H}) \;,\; \dot{\mathbf{H}} = \dot{\lambda}\,\mathbf{h}(\boldsymbol{\sigma};\mathbf{H}) \tag{2}$$

(a) where $\mathbf{C}^e$ is the elastic moduli tensor, $\mathbf{r}$ is the direction of the plastic flow and $\mathbf{h}$ is the direction of the rate of the plastic internal variables $\mathbf{H}$.

❸ The plastic strain rate is decomposed into volumetric and deviatoric parts, $\dot{\boldsymbol{\epsilon}}^p = \frac{1}{3}\,\dot{\epsilon}^p_v\,\mathbb{1} + \dot{\boldsymbol{\epsilon}}^p_q$, which facilitates development of the integration algorithm :

$$\dot{\epsilon}^p_v = -\dot{\lambda}\,\frac{\partial \Phi}{\partial p} \text{ and } \dot{\boldsymbol{\epsilon}}^p_q = \dot{\lambda}\left(\frac{\partial \Phi}{\partial \boldsymbol{\sigma}'} - \frac{2}{9}\,\frac{\partial \Phi}{\partial J_3}\,q^2\,\mathbb{1}\right) \tag{3}$$

(a) The presence of J_3 in the expression of the yield function Φ the deviatoric component $\dot{\boldsymbol{\epsilon}}^p_q$ cannot be put in the form $\dot{\boldsymbol{\epsilon}}^p_q = \dot{\epsilon}^p_q\,\mathbf{n}$, where $\mathbf{n}$ is the deviatoric strain rate tensor normal to the yield surface $\Phi = 0$ and which norm is unity.

(b) To determine the plastic multiplier, the loading unloading conditions should be imposed in a Kuhn-Tucker form as

$$\dot{\lambda} \geq 0, \quad \Phi(p, q, J_3; \mathbf{H}) \leq 0, \quad \dot{\lambda}\,\Phi(p, q, J_3; \mathbf{H}) = 0 \tag{4}$$

implying that during plastic loading, $\Phi = 0$, $\dot{\lambda} \geq 0$ and $\dot{\Phi} = 0$.

❹ The *effective* void volume fraction $f^\star$ proposed by Tvergaard and Needleman (1991) is used to simulate the rapid loss of strength accompanying void coalescence.

- The extended yield function Φ given by (1), the Tvergaard q-like parameters a_1 and a_2 depend on f, that is $a_1 = a_1(f)$, $a_2 = a_2(f)$. It linearly depends upon the third stress invariant I_3 with coefficient proportional to the hydrostatic pressure p. The parameter s, also depending on f, determines the influence of the new term in the yield condition (1) which reduces to that of the classical GTN model for $s = 0$, $a_1 = q_1\,f$ and $a_2 = q_2$.
- Whenever the constant s is non-zero, there is an effect of I_3 on the plastic flow. Clearly the yield function Φ contains three functions of void-volume fraction f, *namely* a_1, a_2 and s which are slightly different for each of the three cubic microstructures considered in [7].
- The calculations have been carried out in Abaqus/Explicit and similar values for the damage parameters have been used for both the proposed model and the GTN one in order to compare their ability to predict void growth to coalescence and the corresponding failure mechanism.

3 Butterfly specimen under shear and tensile loading

Fig. 1 shows a schematic representation of the geometry of the specimen under consideration. It is about the butterfly specimen designed by Bai and Wierzbicki [1] and Mohr and Henn [8]. Its geometry is such that fracture triggers within the flat large central area of the gage section. Consequently, the start failure zone is then remote from the lateral free edges. The butterfly specimen exhibits an abrupt change in thickness between the gage section and its shoulders. The distinctive features of the optimized geometry proposed by Dunand and Mohr [6] is a gage section of reduced thickness bounded by shoulders of clothoid shape. As a result, wide range of stress and strain states within the middle gage section can be displayed by simultaneously loading the top and bottom of the specimen boundaries, horizontally and/or vertically. Hereafter, calculations are performed on steel alloys in order to determine the stress and strain fields within the specimen gage section.

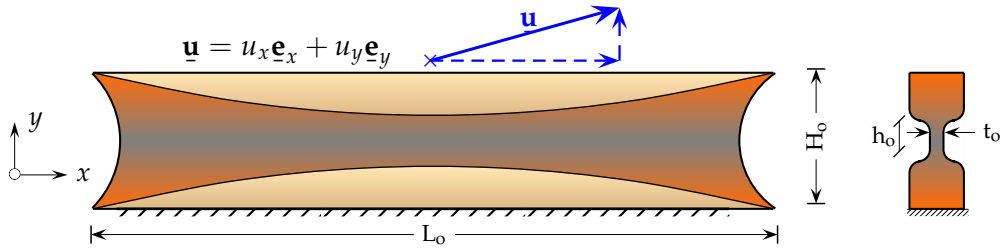

FIGURE 1 – Schematic representation of the geometry and loading of a butterfly specimen, (adapted from Refs. [6, 5])

- **Material parameters and geometrical constants** of the butterfly specimen [5] used in this simulation : $\bar{\sigma}/\sigma_o(\bar{\epsilon}^p) = \left(1 + E\,\bar{\epsilon}^p/\sigma_o\right)^N$, $E/\sigma_o = 300.0$, $\nu = 0.3$, $\mathrm{N} = 0.10$, $\rho = 7830\,\mathrm{kg/m^3}$, $f_o = 0.01$, $q_1 = 1.5$, $q_2 = 1.0$, $q_3 = 2.25$, $f_c = 0.067$, $f_f = 0.20$, $\mathrm{H_o} = 12.6\,\mathrm{mm}$, $\mathrm{L_o} = 62.1\,\mathrm{mm}$, $\mathrm{h_o} = 2.0\,\mathrm{mm}$, $\mathrm{t_o} = 0.4\,\mathrm{mm}$, $5 \times 10^{-3}s \leq$ Time period $\leq 6 \times 10^{-3}s$.
- **Loading conditions** : the bottom face of the specimen $x = -H_o/2$ is maintained fixed, whereas the top face $x = H_o/2$ is subject to a controlled displacement expressed as $\mathbf{u} = u_x\mathbf{e}_x + u_y\mathbf{e}_y$ with $u_x = \alpha\, u_y$, $(0 < \alpha < 1)$ for shear-dominated deformation loading.

Results based on the present constitutive model and the GTN one are compared, for the above stated loading conditions, in order to evaluate the predictive capabilities of the former. The loading paths to fracture of specimens are determined in terms of displacements. For each calculation, (i) tangential force RF_x versus horizontal displacement u_x curves, and (ii) axial force RF_y versus vertical displacement u_y curves. are recorded. Numerous and various loading conditions, ranging from pure shear to transverse plane strain tension, are considered.

4 Discussion and concluding remarks

Fig. 2(a) depicts the force-displacement curves predicted by both models for six loadings ranging from shear-dominated deformation $(\alpha = 0.1)$ to tension-dominated deformation $(\alpha = 0.9)$; including pure shear loading $(\alpha = 0.)$. For the sake of space, Fig. 2(b) only shows the void volume fraction contour corresponding to the almost total failure of the butterfly specimen under a shear-dominated loading corresponding to $\alpha = 0.10$. It should be noted that in all performed calculations, plastic deformation localizes within the gage section prior to fracture. It can be seen from Fig. 2(a) that for high stress triaxiality (tension deformation), the present constitutive model gives quite similar predictions as the GTN model. The $F_y - u_y$ curves exhibit a peak preceding a fast drop of the force, which could occur simultaneously with the onset of localized deformation. For very low stress triaxiality (shear deformation) the behaviour is qualitatively the same ; indeed, up to the failure initiation of the specimen, the predictions incorporating the present model are also in a close agreement with those provided by the GTN model. For shear-dominated deformation, namely $0 \leq \alpha \leq 0.3$, the obtained force-displacement curves display a "plateau" which extent depends

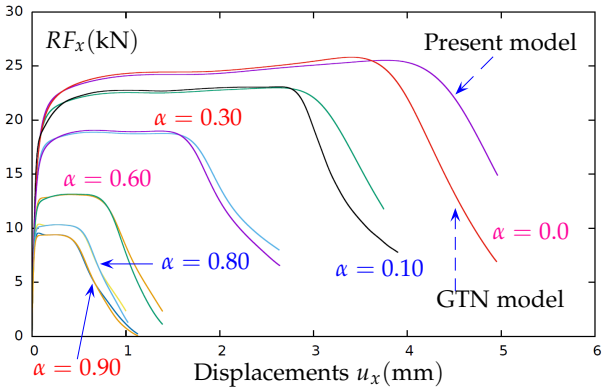

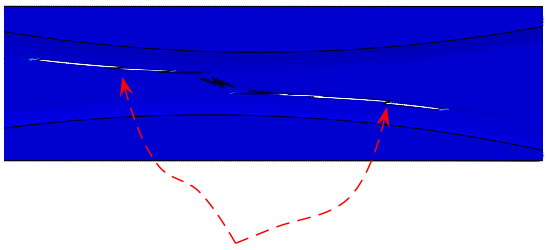

Failed shear bands developed within the central area of the gage section. The shear-dominated loading corresponds to $\alpha = 0.10$.

FIGURE 2 – (a) Comparison of force-displacement curves obtained for both present and GTN constitutive models : the butterfly specimen is subject to various loadings for which the load parameter α ranges from 0.1 (shear-dominated deformation) to 0.9 (tension-dominated deformation). (b) Failure modes under shear-dominated deformation with $\alpha = 0.1$.

on the loading parameter α. Higher the value of this parameter, wider the extent of the "plateau". Significant difference starts at and beyond failure points of specimen.

The main objective of this investigation has been to address an extended version of the GTN model based on a pre-existing yield function for porous plastic materials proposed in [7] and its implementation within a finite element code. To this end, a fully implicit stress integration scheme has been chosen. Similar values for the material parameters (elasticity, hardening, Tvergaard parameters, and coalescence parameters) have been used for both the present model and the GTN model in order to compare their ability to predict fracture of an optimized butterfly specimen [5, 6]. The obtained computational results may be briefly summarized as follows :

- For all performed calculations, using the proposed constitutive model and the GTN model for comparison purpose, plastic deformation localizes within the gage section prior to initiation of fracture faithfully in his zone.
- At high stress triaxialities (tension-dominated deformation), the proposed constitutive model gives similar predictions as the GTN model. Indeed, up to the failure initiation of the specimen, the predictions incorporating the present model are in a close agreement with those provided by the GTN model. This observation insists the potential of the former constitutive model to fulfill to the requirement of transferability between different loading conditions.
- For shear-dominated loading, at and beyond failure points of specimen, noticeable disagreement has been observed between predictions of both models.

References

[1] Y. Bai, T. Wierzbicki, Application of extended Mohr-Coulomb criterion to ductile fracture, International Journal of Fracture, 161 (2010), 1–20.

[2] R. Borja. Plasticity. Modeling and computations Springer, Dordrecht, 2013.

[3] L. Chen and C. Butcher. Micromechanics modelling of ductile fracture, Springer, Dordrecht, 2013.

[4] J.G. Cowie, M. Azrin and G.B. Olson. Microvoid formation during shear deformation of ultrahigh strength steels, Metallurgical Transaction A, 20A (1989), 143–153.

[5] K. Danas, N. Aravas, Numerical modeling of elasto-plastic porous materials with void shape effects at finite deformations, Composites-Part B, 43 (2012) 2544-2559.

[6] M. Dunand, D. Mohr. Optimized butterfly specimen for the fracture testing of sheet materials under combined normal and shear loading, Engineering Fracture Mechanics, 78 (2011), 2919–2934.

[7] D.L. Sean McElwain, A.P. Roberts and A.H. Wilkins. Yield criterion for porous materials sujected to complex stress states, Acta materialia, 54 (2006).

[8] D. Mohr, S. Henn, Calibration of stress-triaxiality dependent crack formation criteria : a new hybrid experimental-numerical method, Exp. Mechanics, 47 (2007), 805–820.